ASTRONOMY & ASTROPHYSICS
SUPPLEMENT SERIES

Astron. Astrophys. Suppl. Ser. **137**, 165–173 (1999)

Atomic data from the IRON Project

XXXVIII. Electron impact excitation of the fine-structure transitions in the $n = 3$ complex of Fe XV*

W. Eissner[1], **M.E. Galavís**[2,4], **C. Mendoza**[3,4], **and C.J. Zeippen**[4]

[1] Fakultät für Physik und Astronomie, Ruhr-Universität, D-44780 Bochum, Germany
[2] Departamento de Física, Universidad Metropolitana, PO Box 76819, Caracas 1070A, Venezuela
[3] Centro de Física, Instituto Venezolano de Investigaciones Científicas (IVIC), PO Box 21827, Caracas 1020A, Venezuela
[4] UMR 8631 (associée au CNRS et à l'Université Paris 7) et DAEC, Observatoire de Paris, F-92195 Meudon, France

Received December 10, 1998; accepted March 2, 1999

Abstract. As part of a systematic study of the collisional properties of Fe ions carried out by the IRON Project, electron excitation rates (effective collision strengths) are computed for all the fine-structure transitions within the $n = 3$ complex of Fe XV in the electron temperature range $10^5 \leq T/K \leq 10^7$. Configuration-interaction target wavefunctions are generated with the atomic structure code SUPERSTRUCTURE, and collision strengths are computed in the close-coupling approximation with a Breit–Pauli R-matrix package. Special care is taken to resolve the resonance structure and to ensure the convergence of the partial wave expansion, specially for dipole allowed transitions. By comparing with previously calculated collision strengths in the distorted wave approximation, a 20% accuracy rating is assigned to transitions with effective collision strengths $\Upsilon(T) > 10^{-2}$.

Key words: atomic data — Sun: corona

1. Introduction

Spectral lines arising from transitions within the $n = 3$ complex of Mg-like Fe XV have been observed in solar active regions, corona and flares as far back as in the earlier pioneering work by Edlén (1942) and then by, among others, Cowan & Widing (1973), Behring et al. (1976), Doschek et al. (1976), Dere (1978, 1982), Vernazza & Reeves (1978), Widing & Cook (1987), Thomas & Neupert (1994) and Brosius et al. (1997a). Furthermore spatially resolved coronal EUV emission-line profiles of Fe XV over a solar active region have been used to detect mass outflow in the low corona (Neupert et al. 1992). Images taken in the 284 Å line have been used by Brueckner (1983) to characterize the coronal magnetic field; and simultaneous observations in the EUV spectrum (including this line) and microwave images allow the mapping of the magnetic field spatial variations suggesting the presence of coronal electric currents (Brosius et al. 1997b). Lines belonging to Fe XV have also been observed in EUV spectra of the Algol eclipsing binary (Stern et al. 1995), of non-supergiant B stars (Cassinelli 1994) and of the nearby K2 dwarf ϵ Eridani (Schmitt et al. 1996).

The usefulness of these lines in devising plasma diagnostics has been extensively discussed (Mason 1975; Kastner & Mason 1978; Dere et al. 1979; Bhatia & Kastner 1980; Dufton et al. 1990; Keenan et al. 1993; Brickhouse et al. 1995). However, the modeled lines are not always in agreement with observations (see, for instance, Dere at al. 1979 and Dufton et al. 1990). The latter authors propose as possible sources of error the exclusion of fluorescence effects or poor atomic data (i.e. poor electron excitation rates due to the neglect of relativistic effects or a limited target representation in the close-coupling calculation). In the case of solar flares Feldman et al. (1992) invoke the direct excitation of the $3s3p\,^3P^o_J$ levels by inner-shell ionisation of the Al-like ion in order to interpret observations; however, the coronal heating rate from bursts obtained from such an approach seems to be larger than the accepted values.

Previous electron impact excitation collision strengths for this ion have been computed at a limited number of energy points by Bhatia & Kastner (1980), Mann (1983), Christensen et al. (CNP, 1985), Bhatia et al. (BMB, 1997)

Send offprint requests to: C.J. Zeippen

* A detailed Table 5 of the present effective collision strengths is only available in electronic form from the CDS via anonymous ftp 130.79.128.5 or via http://cdsweb.u-strasbg.fr/Abstract.html

and Bhatia & Mason (BM, 1997) in the distorted wave approximation. Using the sparse tabulation by Christensen et al., Pradhan (1988) has estimated rate coefficients for a 16-level system in the electron temperature range $4.8 \leq \log(T/K) \leq 7.6$. Rates computed (but not listed) by Dufton et al. (1990) from a 20-point tabulation of collision strengths in an 8-state close-coupling approximation are found to be in excellent agreement ($\sim$20% or better) with those by Pradhan. The common approach adopted in all these calculations implies the assumption, as stated by Dufton et al. and BMB, that the contribution from resonances can be neglected at the high temperatures of the solar medium. The validity of this assumption has never been really tested in the case of Fe XV, in particular for the non-allowed transitions that usually display small background cross sections. Some of these transitions, even though their collisional and radiative rates are considerably smaller than those of their optically allowed counterparts, are nonetheless of astrophysical interest.

In the present work we have calculated effective collision strengths (excitation rates) for the $n = 3$ transitions of Fe XV in the close-coupling approximation (Burke & Seaton 1971). Particular care is taken to resolve the resonance structure and to ensure the convergence of the partial wave expansion which can be tricky for both allowed and forbidden transitions. Relativistic effects are taken into account by means of a Breit–Pauli Hamiltonian. Therefore the present approach should lead to a more reliable collisional dataset for this ion. This work is performed as part of the systematic study of the atomic properties of Fe ions undertaken by the international collaboration known as the IRON Project (Hummer et al. 1993; Butler 1996; Mendoza 1999). A detailed comparison with the work of CNP, BMB, BM and Pradhan (1988) is also carried out in an attempt to assign accuracy ratings to the present dataset. The earlier work by Bhatia & Kastner (1980) and Mann (1983) has already been analysed by CNP and will not be included in the present discussion.

2. Method

The precise approach adopted to compute effective collision strengths for the present system is a legacy of the experience gained in our previous treatment of the excitation by electron impact of Na-like Fe XVI (Eissner et al. 1999). Following the common policy of the IRON Project, the method is based on the close-coupling approximation of Burke & Seaton (1971) as implemented in the R-matrix package of Burke et al. (1971) and Berrington et al. (1974, 1978), with developments in the asymptotic region by Seaton (1985) and Berrington et al. (1987). In this method the wavefunction of the target–electron system is expanded in terms of the target eigenfunctions which are discussed in Sect. 3. Previous work by Dufton et al. (1990) follows a similar method but with a reduced target representation (8-state). The calculations by CNP, BMB and BM have been carried out in the distorted wave approximation that neglects channel coupling.

Collision strengths for the fine-structure levels are calculated including relativistic effects by means of a Breit–Pauli version of the R-matrix codes (Scott & Burke 1980; Scott & Taylor 1982) within an intermediate coupling scheme that leads to intermediate states of the total system with angular momentum and parity quantum numbers $J\pi$. In the work by CNP, BMB, BM and Dufton et al. (1990), collision strengths for the fine-structure levels are computed by an algebraic recoupling of the LS reactance matrices, including relativistic effects in the target by means of term-coupling coefficients (Hummer et al. 1993). This approach, although computationally less involved, is not expected to perform as reliably as a full Breit–Pauli approximation (Eissner et al. 1999).

Due to the important contributions to the collision strengths of optically allowed transitions from the long-range coupling of non-coulombic potentials in the asymptotic region (see Eissner et al. 1999), the present computations are performed taking into account this interaction throughout the partial wave expansion. The occasional appearance of artificially high resonances caused by numerical instabilities is managed by comparing with calculations in the resonance region that exclude this effect, and trimming down any resonance that differs by a factor larger than 5.

The high-l top-up of the collisional strength for optically allowed transitions is computed for $J > J^{\rm oa}_{\rm max}$ with a procedure based on the Coulomb–Bethe approximation (Burgess 1974) as discussed within the context of the close-coupling approximation by Burke & Seaton (1986). The intermediate coupling implementation of this top-up procedure in the R-matrix code was developed by one of us and tested in the study of Fe XVI. The corresponding top-up for non-allowed transitions is approximated for $J > J^{\rm na}_{\rm max}$ with a geometric series sum. Similarly to our earlier work on the Na-like ion, it has also been found that for this system the Coulomb–Born regime in allowed transitions and in some quadrupole transitions is only reached at the high energies ($E > 100$ Ryd, say) when l is very high. It is therefore necessary to take into account an extended partial wave range in the R-matrix calculation in order to ensure a reasonable degree of reliability in the top-up procedures for all the slow converging transitions. In the present work we have settled for $J^{\rm oa}_{\rm max} = J^{\rm na}_{\rm max} = 40.5$. This model contrasts with those adopted by CNP, BMB and BM where a dipole top-up was introduced at $l > 11$ and with that by Dufton et al. (1990) at $l > 8$. Moreover, in these previous calculations the quadrupole top-up has been generally neglected, except by BMB and BM for transitions involving the ground level.

As shown by Eissner et al. (1999) the energy-mesh step size in the resonance region must be carefully considered

due to the complicated structure of narrow features. After some experimentation a step of $\delta e/z^2 = 10^{-5}$ Ryd was selected where $z = 14$ is the effective charge of the system. In the region of all channels open above the highest excitation threshold a broader step of $\delta E/z^2 = 10^{-2}$ Ryd was regarded as adequate. The mesh adopted in previous work was generally coarse, since the resonance contribution to the rates has been assumed to be negligible in the temperature range of interest.

Collision strengths and effective collision strengths are analysed with the scaling techniques developed by Burgess & Tully (1992), in particular the convergence of the partial wave expansion. The collision strength $\Omega(E)$ is mapped onto the reduced form $\Omega_{\rm r}(E_{\rm r})$, where the infinite energy E range is scaled to the finite $E_{\rm r}$ interval $(0, 1)$. For an allowed transition the scaling is given by the relations

$$E_{\rm r} = 1 - \frac{\ln(c)}{\ln(E/\Delta E + c)} \quad (1)$$

$$\Omega_{\rm r}(E_{\rm r}) = \frac{\Omega(E)}{\ln(E/\Delta E + {\rm e})} \quad (2)$$

with ΔE being the transition energy, E the electron energy with respect to the reaction threshold and c is an adjustable scaling parameter. For an electric dipole transition the important limit points are

$$\Omega_{\rm r}(0) = \Omega(0) \quad (3)$$

$$\Omega_{\rm r}(1) = \frac{4gf}{\Delta E} \quad (4)$$

where gf is the weighted oscillator strength for the transition. This method can also be extended to treat the effective collision strength

$$\Upsilon(T) = \int_0^\infty \Omega(E) \exp(-E/\kappa T) {\rm d}(E/\kappa T) \quad (5)$$

through the analogous relations

$$T_{\rm r} = 1 - \frac{\ln(c)}{\ln(\kappa T/\Delta E + c)} \quad (6)$$

$$\Upsilon_{\rm r}(T_{\rm r}) = \frac{\Upsilon(T)}{\ln(\kappa T/\Delta E + {\rm e})} \quad (7)$$

where T is the electron temperature and κ the Boltzmann constant; the limit points remain

$$\Upsilon_{\rm r}(0) = \Omega(0) \quad (8)$$

$$\Upsilon_{\rm r}(1) = \frac{4gf}{\Delta E}\,. \quad (9)$$

Similarly, for a forbidden transition the scaling relations are given by

$$E_{\rm r} = \frac{E/\Delta E}{E/\Delta E + c} \quad (10)$$

$$\Omega_{\rm r}(E_{\rm r}) = \Omega(E) \quad (11)$$

$$T_{\rm r} = \frac{\kappa T/\Delta E}{\kappa T/\Delta E + c} \quad (12)$$

$$\Upsilon_{\rm r}(T_{\rm r}) = \Upsilon(E) \quad (13)$$

with the following limit points:

$$\Omega_{\rm r}(0) = \Omega(0) \quad (14)$$

$$\Omega_{\rm r}(1) = \Omega_{\rm CB} \quad (15)$$

$$\Upsilon_{\rm r}(0) = \Omega(0) \quad (16)$$

$$\Upsilon_{\rm r}(1) = \Omega_{\rm CB} \quad (17)$$

where $\Omega_{\rm CB}$ is the Coulomb–Born high-energy limit.

Caution is required in the use of Eq. (5) to calculate effective collision strengths when $\Omega(E)$ varies rapidly due to the presence of resonances. To ensure the proper behaviour at low temperatures, the integration technique presented by Burgess & Tully (1992) was adopted.

3. Target representation

As shown in Table 1, the Fe XV target contains all the 35 fine-structure levels within the $n = 3$ complex. Configuration interaction (CI) wavefunctions are obtained with the structure code SUPERSTRUCTURE, originally developed by Eissner et al. (1974) with extensions by Nussbaumer & Storey (1978). CI arising from configurations containing orbitals with $n > 3$ is neglected. The one-electron orbitals are generated in a statistical Thomas–Fermi–Dirac-Amaldi model potential $V(\lambda_l)$ described by Eissner & Nussbaumer (1969). The scaling parameters λ_l are computed variationally so as to minimize the sum of the non-relativistic term energies. The optimized parameters for the present calculation are: $\lambda_0 = 1.1256$; $\lambda_1 = 1.0429$; $\lambda_2 = 1.0696$.

In Table 1 we compare the present level energies with experiment (Churilov et al. 1985, 1989; Litzén & Redfors 1987; Redfors 1988) and with the computed results of BM, BMB and CNP. A relevant feature in this level structure has to do with the assignments of the $3d^2\ ^1D_2$ and $^3P_2$ levels ($i = 30$ and $i = 33$, respectively, in Table 1). These two levels are strongly mixed by relativistic couplings up to the point of making unambiguous assignments almost meaningless. The listed assignments are those given by experiment whereas SUPERSTRUCTURE usually inverts them (see, for instance, BM). Furthermore, energy positions for the $3d^2\ ^3P_J$ levels have not been actually measured; the values listed in Table 1 have been obtained by Churilov et al. (1989) by fitting to spectroscopic data, making the order of levels 33 and 34 somewhat uncertain. For this reason they are treated in the present computations as degenerate.

The agreement between present level energies and the measured values is better than 1% except for the $3p3d\ ^1F^{\rm o}_3$ and $^1P^{\rm o}_1$ where it deteriorates to $\sim 2\%$. The target used by BM (see Table 1) is very similar to the present one thus leading to very close level energies. The target selected by BMB includes the 78 levels from the following configurations: $3s^2$, 3s3p, $3p^2$, 3s3d, 3p3d, 3s4l and 3p4l. A notable exclusion in this ansatz is the important $3d^2$ configuration which thus results in a poorly represented $3p^2\ ^1S_0$ level,

Table 1. Comparison of experimental and theoretical energy levels (Rydberg units) for the Fe XV target. Expt: Churilov et al. (1985, 1989), Litzén & Redfors (1987) and Redfors (1988). Pres: present results. BM: Bhatia & Mason (1997). BMB: Bhatia et al. (1997). CNP: Christensen et al. (1985)

i	Level	Expt	Pres	BM	BMB	CNP
1	$3s^2\ ^1S_0$	0.000	0.000	0.000	0.000	0.000
2	$3s3p\ ^3P^o_0$	2.131	2.126	2.126	2.112	2.120
3	$3s3p\ ^3P^o_1$	2.184	2.177	2.177	2.165	2.172
4	$3s3p\ ^3P^o_2$	2.313	2.298	2.298	2.289	2.296
5	$3s3p\ ^1P^o_1$	3.207	3.245	3.245	3.240	3.239
6	$3p^2\ ^3P_0$	5.053	5.074	5.074	5.093	5.068
7	$3p^2\ ^1D_2$	5.100	5.105	5.105	5.106	5.101
8	$3p^2\ ^3P_1$	5.145	5.158	5.158	5.176	5.154
9	$3p^2\ ^3P_2$	5.302	5.303	5.304	5.322	5.303
10	$3p^2\ ^1S_0$	6.011	6.056	6.057	6.227	6.056
11	$3s3d\ ^3D_1$	6.186	6.225	6.226	6.212	6.213
12	$3s3d\ ^3D_2$	6.195	6.236	6.237	6.224	6.225
13	$3s3d\ ^3D_3$	6.210	6.254	6.254	6.241	6.242
14	$3s3d\ ^1D_2$	6.945	7.062	7.064	7.089	7.013
15	$3p3d\ ^3F^o_2$	8.459	8.494	8.494	8.485	
16	$3p3d\ ^3F^o_3$	8.549	8.581	8.581	8.571	
17	$3p3d\ ^1D^o_2$	8.644	8.674	8.674	8.668	
18	$3p3d\ ^3F^o_4$	8.654	8.680	8.680	8.671	
19	$3p3d\ ^3D^o_1$	8.957	9.012	9.013	9.007	
20	$3p3d\ ^3P^o_2$	8.963	9.018	9.019	9.013	
21	$3p3d\ ^3D^o_3$	9.065	9.119	9.121	9.115	
22	$3p3d\ ^3P^o_0$	9.075	9.121	9.122	9.116	
23	$3p3d\ ^3P^o_1$	9.079	9.126	9.127	9.121	
19	$3p3d\ ^3D^o_2$	9.081	9.132	9.133	9.127	
25	$3p3d\ ^1F^o_3$	9.682	9.830	9.832	9.793	
26	$3p3d\ ^1P^o_1$	9.794	9.944	9.947	9.937	
27	$3d^2\ ^3F_2$	12.488	12.552	12.553		
28	$3d^2\ ^3F_3$	12.503	12.570	12.571		
29	$3d^2\ ^3F_4$	12.521	12.592	12.594		
30	$3d^2\ ^1D_2$	12.783	12.879	12.881		
31	$3d^2\ ^3P_0$	12.808	12.882	12.882		
32	$3d^2\ ^3P_1$	12.814	12.889	12.889		
33	$3d^2\ ^3P_2$	12.822	12.914	12.915		
34	$3d^2\ ^1G_4$	12.822	12.957	12.958		
35	$3d^2\ ^1S_0$	13.551	13.714	13.715		

Table 2. Comparison of theoretical radiative rates A_{ij} (s^{-1}) for transitions to the lowest five levels of the Fe XV target. Pres: present results. BM: Bhatia & Mason (1997). BMB: Bhatia et al. (1997). CNP: Christensen et al. (1985). ($a+b \equiv a\times 10^b$)

i	j	Pres	BM	BMB	CNP
3	1	3.759+7	3.751+7	3.585+7	3.79+7
5	1	2.326+10	2.323+10	2.265+10	2.22+10
8	2	7.190+9	7.178+9	7.281+9	6.95+9
11	2	1.453+10	1.456+10	1.420+10	1.38+10
6	3	1.871+10	1.866+10	1.896+10	1.79+10
7	3	1.112+9	1.104+9	9.771+8	1.11+9
8	3	5.097+9	5.086+9	5.151+9	4.90+9
9	3	4.607+9	4.608+9	4.829+9	4.48+9
10	3	2.954+8	2.942+8	1.871+8	2.77+8
11	3	1.044+10	1.046+10	1.020+10	9.90+9
12	3	1.897+10	1.900+10	1.855+10	1.80+10
14	3	3.142+8	3.158+8	3.312+8	2.97+8
7	4	2.061+9	2.043+9	1.732+9	2.00+9
8	4	7.511+9	7.495+9	7.550+9	7.16+9
9	4	1.317+10	1.317+10	1.366+10	1.27+10
11	4	6.389+8	6.389+8	6.245+8	6.02+8
12	4	5.818+9	5.826+9	5.694+9	5.49+9
13	4	2.341+10	2.345+10	2.294+10	2.21+10
14	4	1.198+7	1.214+7	1.472+7	1.27+7
6	5	5.571+7	5.536+7	3.802+7	6.19+7
7	5	1.525+9	1.521+9	1.501+9	1.58+9
8	5	7.430+6	7.405+6	7.489+6	8.39+6
9	5	4.567+8	4.526+8	3.853+8	4.83+8
10	5	2.002+10	1.998+10	2.424+10	2.02+10
11	5	2.268+7	2.270+7	2.310+7	2.56+7
12	5	1.617+7	1.653+7	1.778+7	1.61+7
14	5	4.460+10	4.465+10	4.594+10	4.22+10

e.g. incorrect energy position above the $3s3d\ ^3D_2$ level (see Table 1). The target by CNP contains the 14 levels that arise from the $3s^2$, 3s3p, $3p^2$, 3s3d configurations and two additional levels from 3s4s; they also take into account extensive CI with configurations including orbitals with $n = 4$ and $n = 5$. All their level energies agree to better than 1% with experiment.

Following BM, computed A-values for transitions to the lowest five levels of Fe XV are compared in Table 2. The agreement between present data and those by BM is as expected very good (within 2%). The comparison with CNP is also satisfactory: 89% of the A-values agree to within 10%, only finding differences of ∼13% for the $8-5$, $6-5$ and $11-5$ transitions. The comparison with BMB, on the other hand, is less favourable as only 74% agree to 10%; large discrepancies (up to 37%) are found for transitions involving the $3p^2\ ^1S_0$ level ($10-3$, $10-5$) and transitions involving the 3s3p configuration ($7-3$, $7-4$, $14-4$, $6-5$, $9-5$). A poor level of agreement is also found with BMB in a more extensive comparison with their listed gf-values (see Table 3) where only 70% agree to within 10%. Moreover, by running a structure calculation with the same target as BMB (same configurations and λ_l parameters) but now including the $3d^2$ configuration, the numbers of gf-values within the 10% accord goes up to 94% (see Table 3); larger differences are now only found for transitions with very small gf-values, e.g. $19-1$, $23-1$, $26-1$, $23-6$, $23-10$ and $23-14$. This finding has two important implications; firstly, by excluding the $3d^2$ configuration BMB have weakened the general reliability of their target and, secondly, the neglect of CI from the $n = 4$ complex in our target does not seem to lead to major consequences.

Table 3. Theoretical weighted oscillator strengths $g_i f_{ij}$ (length formulation) for the Fe XV target. Pres1: present results. BMB: Bhatia et al. (1997). Pres2: structure calculation with the same target as BMB but including the $3d^2$ configuration. ($a \pm b \equiv a \times 10^{\pm b}$)

j	i	Pres1	BMB	Pres2	j	i	Pres1	BMB	Pres2	j	i	Pres1
3	1	2.962−3	2.857−3	2.933−3	20	12	3.796−2	3.983−2	3.996−2	28	24	8.212−1
5	1	8.251−1	8.058−1	8.164−1	20	13	6.772−1	6.518−1	6.513−1	28	25	3.213−3
6	3	2.775−1	2.754−1	2.721−1	20	14	5.118−3	3.002−3	4.922−3	29	16	1.554−2
6	5	2.072−3	1.379−3	2.124−3	21	7	3.923−1	3.549−1	3.956−1	29	18	1.142+0
7	3	8.079−2	7.030−2	8.172−2	21	9	1.569+0	1.676+0	1.528+0	29	21	2.220+0
7	4	1.629−1	1.359−1	1.620−1	21	12	1.886−1	1.840−1	1.845−1	29	25	9.820−4
7	5	2.744−1	2.682−1	2.694−1	21	13	8.515−1	8.385−1	8.381−1	30	3	1.424−4
8	2	2.922−1	2.898−1	2.877−1	21	14	3.380−3	3.640−3	3.497−3	30	4	1.046−4
8	3	2.142−1	2.122−1	2.106−1	22	8	1.724−1	1.986−1	1.696−1	30	5	1.707−3
8	4	3.430−1	3.384−1	3.357−1	22	11	1.732−1	1.661−1	1.661−1	30	15	8.976−2
8	5	7.579−4	7.464−4	7.444−4	23	1	4.770−7	2.816−7	3.934−7	30	16	6.740−3
9	3	2.935−1	3.016−1	2.876−1	23	6	1.895−4	1.413−3	3.139−4	30	17	7.807−1
9	4	9.080−1	9.245−1	8.906−1	23	7	3.615−2	3.494−2	3.615−2	30	19	3.770−2
9	5	6.710−2	5.533−2	6.746−2	23	8	3.760−1	4.089−1	3.672−1	30	20	7.297−2
10	3	2.444−3	1.412−3	2.457−3	23	9	1.880−1	2.200−1	1.848−1	30	21	2.500−1
10	5	3.153−1	3.383−1	3.162−1	23	10	2.471−5	7.929−6	1.986−5	30	23	1.680−1
11	2	3.231−1	3.156−1	3.156−1	23	11	3.642−1	3.522−1	3.523−1	30	24	3.185−1
11	3	2.380−1	2.326−1	2.326−1	23	12	1.388−1	1.331−1	1.332−1	30	25	1.307−1
11	4	1.547−2	1.515−2	1.515−2	23	14	3.331−5	3.471−5	3.727−5	30	26	3.534−1
11	5	9.534−4	9.764−4	9.856−4	24	7	1.165−1	1.056−1	1.159−1	31	3	8.214−5
12	3	7.166−1	7.008−1	7.010−1	24	8	2.071−1	1.935−1	1.978−1	31	5	3.161−6
12	4	2.335−1	2.289−1	2.289−1	24	9	8.307−1	9.383−1	8.168−1	31	19	3.573−1
12	5	1.125−3	1.243−3	1.171−3	24	11	1.188−1	1.153−1	1.153−1	31	23	9.825−2
13	4	1.304+0	1.280+0	1.280+0	24	12	5.784−1	5.640−1	5.636−1	31	26	1.026−3
14	3	8.198−3	8.504−3	8.233−3	24	13	1.058−1	1.016−1	1.017−1	32	2	1.096−4
14	4	3.288−4	3.978−4	3.571−4	24	14	7.050−4	3.210−4	6.607−4	32	3	7.590−5
14	5	1.906+0	1.931+0	1.887+0	25	7	8.632−1	9.035−1	8.828−1	32	4	8.130−5
15	7	1.118−1	1.175−1	1.063−1	25	9	2.206−1	2.006−1	2.345−1	32	5	9.581−9
15	8	1.604−3	1.657−3	1.637−3	25	12	2.293−3	2.065−3	2.164−3	32	15	1.182−4
15	9	7.886−3	5.986−3	7.643−3	25	13	8.145−3	8.572−3	8.655−3	32	17	2.341−2
15	11	4.087−1	3.942−1	3.938−1	25	14	2.220+0	2.148+0	2.049+0	32	19	4.985−4
15	12	1.084−1	1.040−1	1.046−1	26	1	7.076−4	3.129−3	1.444−3	32	20	6.826−1
15	13	1.675−3	1.697−3	1.692−3	26	6	3.979−3	3.166−3	4.115−3	32	22	3.217−1
15	14	2.018−2	1.179−2	1.853−2	26	7	6.629−3	4.154−3	6.699−3	32	23	3.352−1
16	7	9.015−3	9.010−3	9.577−3	26	8	9.375−4	8.887−4	9.198−4	32	24	1.227−3
16	9	9.083−3	9.861−3	8.666−3	26	9	1.595−3	8.495−4	1.607−3	32	26	8.576−6
16	12	6.983−1	6.691−1	6.686−1	26	10	6.735−1	8.236−1	6.734−1	33	3	2.938−5
16	13	1.502−1	1.442−1	1.445−1	26	11	8.857−4	8.898−4	8.978−4	33	4	2.380−4
16	14	3.613−3	3.609−3	3.676−3	26	12	3.605−3	3.491−3	3.549−3	33	5	1.458−3
17	7	7.628−1	8.474−1	7.565−1	26	14	6.325−1	7.020−1	5.981−1	33	15	3.486−2
17	8	2.336−2	2.543−2	2.335−2	27	3	2.466−7			33	16	8.098−4
17	9	9.407−2	7.921−2	9.544−2	27	4	9.817−8			33	17	3.068−1
17	11	5.660−2	5.188−2	5.194−2	27	5	3.417−8			33	19	2.545−2
17	12	1.190−2	1.143−2	1.105−2	27	15	6.151−1			33	20	3.062−1
17	13	2.806−2	2.679−2	2.708−2	27	16	7.858−2			33	21	2.785−1
17	14	1.688−1	1.056−1	1.630−1	27	17	6.367−2			33	23	1.827−1
18	13	1.136+0	1.088+0	1.088+0	27	19	7.737−1			33	24	6.226−1
19	1	1.783−7	3.734−6	2.842−7	27	20	5.963−2			33	25	1.382−1
19	6	6.525−1	6.949−1	6.395−1	27	21	1.875−3			33	26	2.979−1
19	7	8.737−4	1.087−3	8.488−4	27	23	2.460−1			34	16	9.668−3
19	8	1.135−1	1.119−1	1.122−1	27	24	8.019−2			34	18	1.263−3
19	9	8.367−3	1.080−2	8.043−3	27	25	1.572−3			34	21	5.553−3
19	10	1.770−3	5.344−4	1.817−3	27	26	1.007−3			34	25	2.913+0
19	11	1.005−1	1.016−1	1.015−1	28	4	1.229−6			35	3	2.918−6
19	12	3.461−1	3.344−1	3.343−1	28	15	3.540−2			35	5	1.446−3
19	14	3.474−3	3.936−3	3.294−3	28	16	8.849−1			35	19	3.420−3
20	7	6.520−3	6.640−3	6.547−3	28	17	2.760−4			35	23	2.022−5
20	8	1.046+0	1.126+0	1.031+0	28	18	7.581−2			35	26	5.610−1
20	9	5.032−2	6.404−2	4.891−2	28	20	7.205−1					
20	11	4.539−2	4.506−2	4.522−2	28	21	1.198−1					

Table 4. Comparison of collision strengths Ω_{ij} for Fe XV for transitions with $j < 15$ at an incident electron energy of 50 Ryd. Some transitions with small collision strengths have been excluded. Pres: present results. BM: Bhatia & Mason (1997). BMB: Bhatia et al. (1997). CNP: Christensen et al. (1985). (Note: the data for the latter were computed at $E = 50.38$ Ryd. $a \pm b \equiv a \times 10^{\pm b}$)

i	j	Pres	BM	BMB	CNP	i	j	Pres	BM	BMB	CNP
1	2	8.407−4	8.140−4	8.310−4	8.22−4	5	6	2.325−2	2.414−2	1.627−2	2.57−2
1	3	2.845−2	2.908−2	2.893−2	2.91−2	5	7	2.929+0	3.017+0	2.972+0	2.85+0
1	4	4.195−3	4.031−3	4.093−3	4.06−3	5	8	1.042−2	1.075−2	1.066−2	1.14−2
1	5	4.176+0	4.135+0	4.117+0	4.05+0	5	9	6.254−1	6.397−1	5.306−1	6.19−1
1	7	9.653−2	9.932−2	1.068−1	7.53−2	5	10	1.910+0	1.961+0	1.960+0	1.99+0
1	9	2.063−2	2.137−2	1.996−2	1.64−2	5	11	9.042−3	9.173−3	9.354−3	9.73−3
1	11	2.177−3	2.074−3	2.083−3	2.12−3	5	12	1.248−2	1.251−2	1.306−2	1.20−2
1	12	3.662−3	3.482−3	3.493−3	3.56−3	5	13	8.286−3	8.000−3	8.001−3	8.01−3
1	13	5.089−3	4.840−3	4.858−3	4.95−3	5	14	7.572+0	7.705+0	7.841+0	7.24+0
1	14	2.282−1	2.245−1	2.267−1	1.71−1	6	7	4.134−2	3.553−2	2.919−2	3.42−2
2	3	6.824−3	6.508−3	6.678−3	6.55−3	6	8	7.859−3	6.790−3	6.987−3	7.07−3
2	4	1.046−1	9.189−2	9.153−2	8.51−2	6	9	5.981−2	5.097−2	5.602−2	4.78−2
2	5	9.990−4	9.850−4	1.014−3	9.89−4	6	10	1.150−4	1.210−4	1.300−4	1.37−4
2	6	5.755−4	5.420−4	5.380−4	5.45−4	6	12	1.975−3	2.190−4	2.600−5	8.17−4
2	7	2.817−3	2.666−3	2.692−3	2.74−3	6	14	3.094−3	2.543−3	2.464−3	2.14−3
2	8	1.613+0	1.625+0	1.617+0	1.58+0	7	8	4.308−2	3.749−2	3.324−2	3.64−2
2	11	1.164+0	1.171+0	1.167+0	1.12+0	7	9	1.894−1	1.630−1	1.393−1	1.54−1
2	12	2.229−3	1.900−3	1.936−3	2.05−3	7	10	1.959−1	1.660−1	1.575−1	1.54−1
2	13	1.439−2	1.322−2	1.341−2	1.33−2	7	11	1.476−3	1.357−3	1.556−3	1.47−3
2	14	9.297−4	9.030−4	9.360−4	9.80−4	7	12	2.923−3	2.274−3	2.611−3	2.56−3
3	4	2.422−1	2.134−1	2.128−1	1.97−1	7	13	4.517−3	3.282−3	3.649−3	3.83−3
3	5	5.937−3	5.321−3	5.445−3	5.37−3	7	14	3.793−2	1.810−2	1.790−2	1.87−2
3	6	1.635+0	1.650+0	1.642+0	1.66+0	8	9	1.860−1	1.586−1	1.628−1	1.49−1
3	7	4.725−1	4.755−1	4.200−1	4.62−1	8	10	6.018−4	6.350−4	6.150−4	6.64−4
3	8	1.214+0	1.223+0	1.216+0	1.20+0	8	11	3.326−3	3.420−4	4.400−5	1.30−3
3	9	1.551+0	1.566+0	1.613+0	1.46+0	8	13	2.976−3	3.580−4	4.800−5	1.23−3
3	10	9.868−3	9.798−3	5.527−3	9.91−3	8	14	1.633−3	1.598−3	1.982−3	1.75−3
3	11	8.748−1	8.815−1	8.790−1	8.63−1	9	10	5.819−2	4.959−2	3.854−2	4.76−2
3	12	2.634+0	2.651+0	2.644+0	2.46+0	9	11	1.186−3	4.330−4	3.210−4	7.33−4
3	13	3.189−2	2.912−2	2.956−2	2.94−2	9	12	4.063−3	9.640−4	5.630−4	2.02−3
3	14	2.561−2	2.563−2	2.680−2	2.47−2	9	13	8.492−3	1.368−3	8.060−4	3.26−3
4	5	6.808−3	6.565−3	6.717−3	6.58−3	9	14	7.810−3	4.488−3	4.739−3	5.11−3
4	6	7.493−4	3.720−4	4.020−4	6.80−4	10	12	3.057−4	2.570−4	1.520−4	2.48−4
4	7	1.004+0	1.016+0	8.660−1	1.01+0	10	13	2.541−4	2.340−4	1.200−4	1.95−4
4	8	2.057+0	2.080+0	2.063+0	2.12+0	10	14	1.069−1	8.411−2	1.012−1	6.68−2
4	9	5.075+0	5.131+0	5.241+0	4.97+0	11	12	1.148−1	1.011−1	1.013−1	9.63−2
4	10	1.142−3	1.071−3	1.031−3	1.11−3	11	13	2.633−2	2.466−2	2.387−2	2.31−2
4	11	8.606−2	8.448−2	8.473−2	8.61−2	11	14	7.185−3	7.338−3	6.992−3	7.26−3
4	12	9.231−1	9.292−1	9.288−1	9.01−1	12	13	1.436−1	1.277−1	1.273−1	1.19−1
4	13	4.976+0	5.015+0	5.014+0	4.48+0	12	14	1.197−2	1.219−2	1.162−2	1.21−2
4	14	5.574−3	5.409−3	5.719−3	5.93−3	13	14	1.677−2	1.701−2	1.618−2	1.68−2

4. Results

Since previous work by CNP, BMB and BM was mainly concerned with the computing of collision strengths, we have made fairly extensive comparisons in terms of this quantity in an attempt to assign an accurate rating to the present effective collision strength dataset. Following BM, we compare collision strengths at the incident electron energy of 50 Ryd (Table 4). In general it is found that present data are slightly larger than those by BM, BMB and CNP, in particular for transitions with small collision strengths; this seems to indicate that the partial wave convergence of the present dataset has been accomplished more thoroughly. Nonetheless the agreement of BM and CNP with the present dataset is very reasonable as 84% of the transitions agree to better than 20%. Larger differences are found with BMB where this level of agreement is only met by 76% of the compared transitions. Further comparisons with the work by BM is not possible as they do not list collision strengths at other energies.

Differences with the datasets by CNP and BMB arise due to partial wave convergence problems that show up mainly in the quadrupole transitions. This situation is clearly illustrated in Fig. 1. BMB have

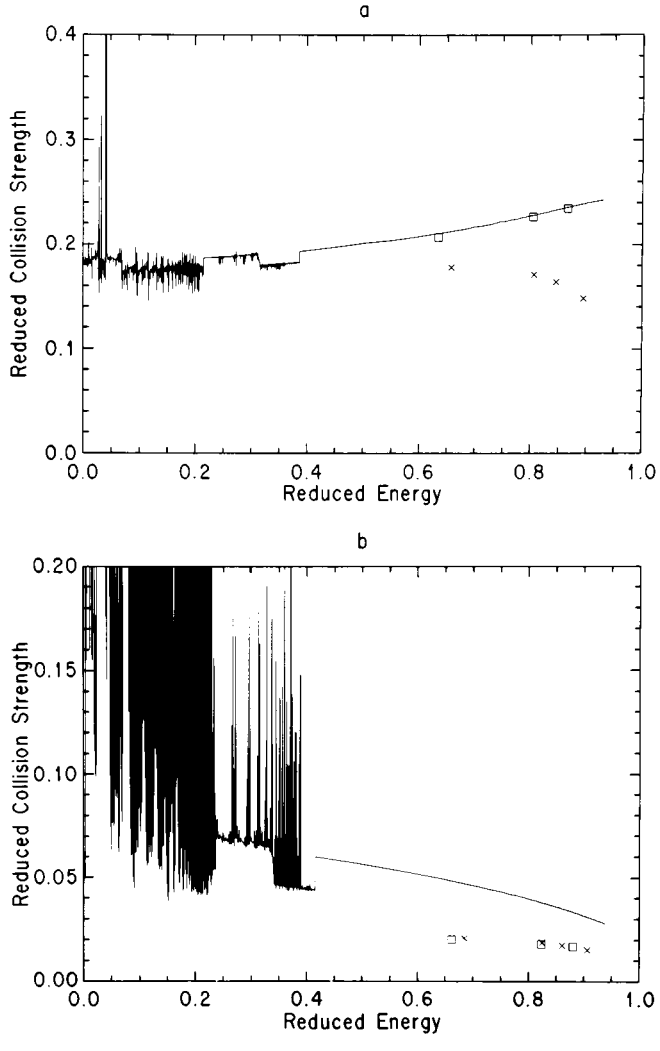

Fig. 1. Collision strength plotted in the reduced scale of Burgess & Tully (1992) for the quadrupole transitions **a)** $3s^2\,{}^1S_0 - 3s3d\,{}^1D_2$ and **b)** $3p^2\,{}^1D_2 - 3s3d\,{}^1D_2$. Solid line, present results; squares, BMB; crosses, CNP. The significant discrepancies found with respect to present results are believed to be caused by the neglect of the contributions from high partial waves

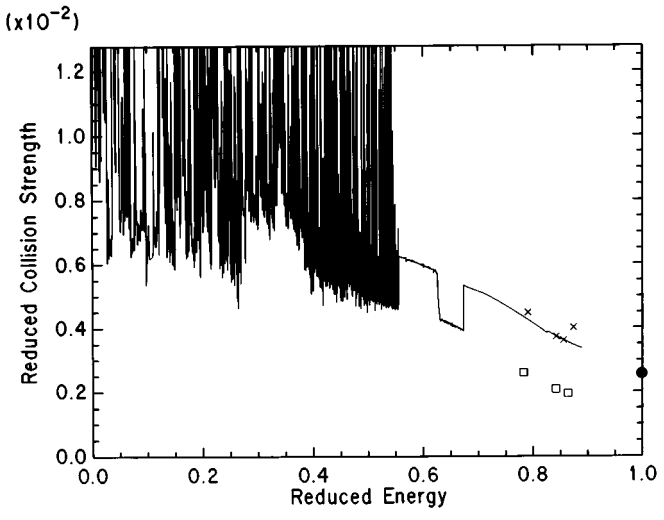

Fig. 2. Reduced collision strength for the $3s3p\,{}^3P^o_1 - 3p^2\,{}^1S_0$ intercombination transition. Solid line: present results. Squares: BMB. Crosses: CNP. Filled circle: high-energy limit. The discrepancies found between BMB and present results are probably due to a poorly represented $3p^2\,{}^1S_0$ in the former work

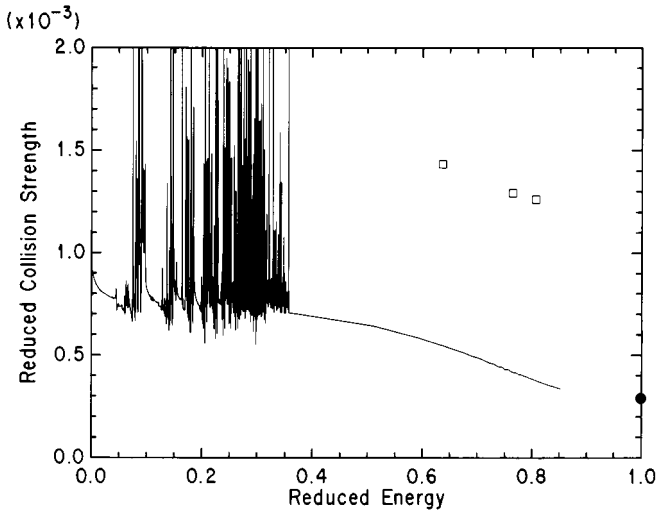

Fig. 3. Reduced collision strength for the $3s^2\,{}^1S_0 - 3p3d\,{}^1P^o_1$ allowed transition. Solid line, present results; squares, BMB; filled circle, high-energy limit. The discrepancies with BMB are due to a small and correlation sensitive gf-value for this transition (see Table 3)

taken into account the contributions from $12 \le l \le 40$ with the non-exchange package NELMA (Cornille et al. 1992) only for transitions arising from the ground level. Therefore the agreement is satisfactory for transition $1 - 14$ ($3s^2\,{}^1S_0 - 3s3d\,{}^1D_2$) but discrepant by a factor of $\sim$2 for transition $7 - 14$ ($3p^2\,{}^1D_2 - 3s3d\,{}^1D_2$). For the same reason, an even bigger difference of a factor of one hundred is noted for transition $6 - 12$ whose collision strength happens to be small. Since CNP neglected contributions from $l > 11$ for all non-dipole transitions, discrepancies are encountered in all three cases. Similar differences (38%) are also found with the values quoted by CNP for the quadrupole transitions $10 - 14$ and, to a lesser extent ($< 25\%$), $1 - 7$, $1 - 9$ and $7 - 10$ (see Table 4).

Noticeable differences are also found with the collision strengths calculated by BMB for some transitions involving the $3p^2\,{}^1S_0$ level, which in their case, as discussed above, is poorly represented due to the exclusion of correlation from the $3d^2$ configuration. In Fig. 2 the present collision strength for the $3s3p\,{}^3P^o_1 - 3p^2\,{}^1S_0$ intercombination transition is plotted using the reduced scale of Burgess & Tully (1992), which shows the correct approach of its high-energy tail towards $\Omega_r(1)$; a discrepancy with BMB of $\sim$40% can be seen. A similar problem is also found for the transition $3p^2\,{}^3P_2 - 3p^2\,{}^1S_0$.

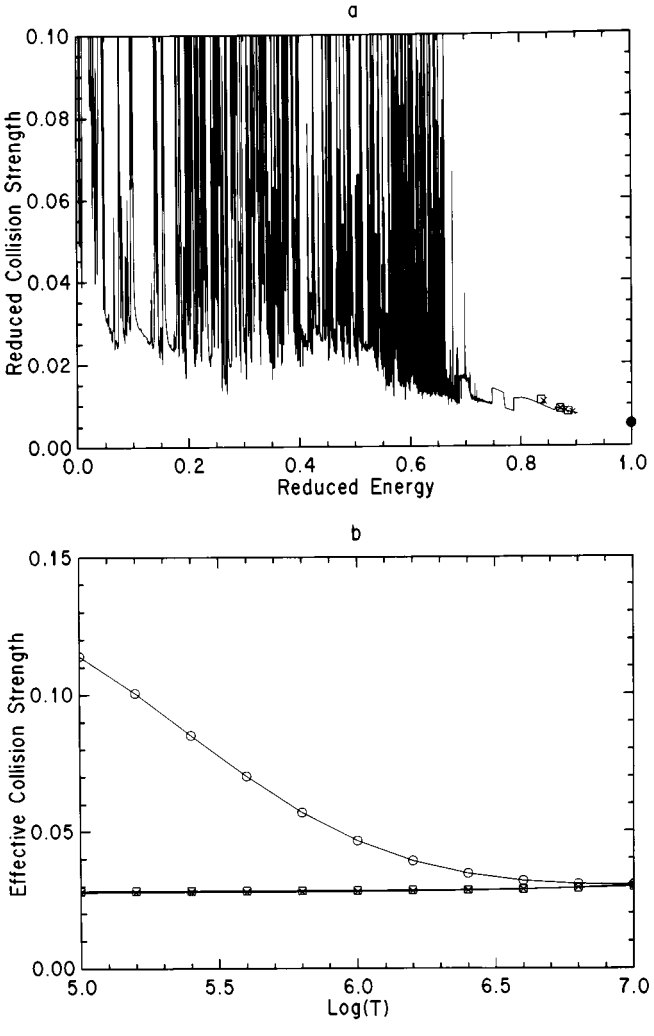

Fig. 4. a) Reduced collision strength for the $3s^2\,{}^1S_0 - 3s3p\,{}^3P^o_1$ intercombination transition showing the complicated resonance structure. Solid line: present results. Filled circle, high-energy limit. **b)** Effective collision strength as a function of electron temperature for this transition. Circles: present results. The results by BMB (squares) and CNP (crosses) are also included, which help to denote the large rate enhancement at the lower temperatures caused by the resonance contribution

In Fig. 3 we plot the present reduced collision strength for the $3s^2\,{}^1S_0 - 3p3d\,{}^1P^o_1$ allowed transition which is in substantial disagreement with BMB. The source of this problem is linked to the large difference in the gf-values (a factor of 4) for this transition (see Table 3). By running several structure calculations, it is found that the gf-value for this transition is sensitive to configuration interaction (see Table 3); a more precise gf-value is probably not as large as that listed by BMB but certainly considerably higher than the present. Thus we would not expect our effective collision strengths for this weak transition to be more accurate than a factor of 2. A similar but less pronounced ($\sim$ 30%) effect is also found in the case of the $3s3p\,{}^1P^o_1 - 3p^2\,{}^3P_0$ intercombination transition.

Effective collision strengths for all the transitions within the present Fe XV target in the electron-temperature range $10^5 - 10^7$ K are tabulated in Table 5. An effect that will influence the rates for some transitions with small backgrounds, e.g. the $3s^2\,{}^1S_0 - 3s3p\,{}^3P^o_1$ intercombination transition, is depicted in Fig. 4. While the tail of the present reduced collision strength displays the correct approach towards the small high-energy limit and is in good agreement with BMB and CNP, the low-energy regime is dominated by the resonance structure (Fig. 4a). By fitting the collision strengths of BMB and CNP to straight lines and estimating effective collision strengths, it is shown in Fig. 4b that the resonance contribution causes a large enhancement in the present results that is conspicuous even at fairly high temperatures; at an electron temperature of $T = 10^6$ K present rates are 40% higher than both BMB and CNP increasing to a factor of 4 at $T = 10^5$ K. This sort of sizable increases due to resonances in some transitions in the solar temperature range justifies the use of the computationally involved close-coupling approximation for highly ionised ions such as Fe XV. This statement is further supported by a comparison of the present effective collision strengths with those listed by Pradhan (1988) estimated from the data by CNP. It is found that only 30% of his data agree with the present ones to within 20%.

5. Discussion

We report for the first time electron impact excitation rates computed in the close-coupling approximation for all the fine-structure transitions within the $n = 3$ complex of Fe XV. Important effects that influence the rate accuracy have been studied and taken into account; that is, target representation, the resonance structure, the convergence of the partial wave expansion, top-up procedures, asymptotic long-range potential couplings and the energy-mesh step. This effort has resulted in a considerable improvement over previous work, which had been mainly carried out with the simpler distorted wave approximation. As shown, relevant effects were sometimes overlooked in previous work hence limiting the overall reliability of the available collisional datasets. However, from extensive comparisons we have attempted to evaluate the accuracy of the present results. We are confident that the listed effective collision strengths with magnitudes $\Upsilon(T) > 10^{-2}$ are accurate to better than 20% whereas those with smaller values are probably reliable only within a factor of 2. We have also demonstrated that excitation rates for highly ionised systems, e.g. Fe XV, obtained from sparsely tabulated collision strengths that do not resolve the resonance structure can be unreliable, and therefore standing inconsistencies in plasma diagnostics at high temperatures in many situations can indeed be due to poor atomic data.

Acknowledgements. Part of the present work was carried out during visits by MEG and CM to the Observatoire de Paris, Meudon, France. The hospitality received is gratefully acknowledged. The visits were funded by the CNRS, IVIC, CONICIT, Fundación Polar, the Observatoire de Paris and the Ministère des Affaires Étrangères. Computations were carried out at the Ohio Supercomputer Center, Columbus, Ohio, U.S.A., and at CeCalCULA, Universidad de Los Andes, Mérida, Venezuela. This research has been supported by CONICIT under contract No. S1-95000521.

References

Behring W.E., Cohen L., Feldman U., Doschek G.A., 1976, ApJ 203, 521
Berrington K.A., Burke P.G., Butler K., Seaton M.J., Storey P.J., Taylor K.T., Yu Y., 1987, J. Phys. B 20, 6379
Berrington K.A., Burke P.G., Chang J.J., Chivers A.T., Robb W.D., Taylor K.T., 1974, Comput. Phys. Commun. 8, 149
Berrington K.A., Burke P.G., Le Dourneuf M., Robb W.D., Taylor K.T., Vo Ky L., 1978, Comput. Phys. Commun. 14, 367
Bhatia A.K., Kastner S.O., 1980, Sol. Phys. 65, 181
Bhatia A.K., Mason H.E., 1997, At. Data Nucl. Data Tab. 66, 119
Bhatia A.K., Mason H.E., Blancard C., 1997, At. Data Nucl. Data Tab. 66, 83
Brickhouse N.S., Raymond J.C., Smith B.W., 1995, ApJS 97, 551
Brosius J.W., Davila J.M., Thomas R.J., Saba J.L.R., Hara H., Monsignori-Fossi B.C., 1997a, ApJ 477, 969
Brosius J.W., Davila J.M., Thomas R.J., White S.M., 1997b, ApJ 488, 488
Brueckner G.E., 1983, Sol. Phys. 85, 243
Burgess A., 1974, J. Phys. B 7, L364
Burgess A., Tully J.A., 1992, A&A 254, 436
Burke P.G., Hibbert A., Robb W.D., 1971, J. Phys. B 4, 153
Burke P.G., Seaton M.J., 1971, Meth. Comput. Phys. 10, 1
Burke V.M., Seaton M.J., 1986, J. Phys. B 19, L527
Butler K., 1996, Phys. Scr. T65, 63
Cassinelli J.P., 1994, Ap&SS 221, 277
Christensen R.B., Norcross D.W., Pradhan A.K., 1985, Phys. Rev. A 32, 93
Churilov S.S., Kononov E.Ya., Ryabtsev A.N., Zayikin Yu.F., 1985, Phys. Scr. 32, 501
Churilov S.S., Levashov V.E., Wyart J.F., 1989, Phys. Scr. 40, 625
Cornille M., Dubau J., Mason H.E., Blancard C., Brown W., 1992, in UV, X-Ray Spectroscopy of Astrophysical and Laboratory Plasmas, Silver E.H. & Kahn S.M. (eds.). Cambridge Univ. Press, Cambridge, UK
Cowan R.D., Widing K.G., 1973, ApJ 180, 285
Dere K.P., 1978, ApJ 221, 1062
Dere K.P., 1982, Sol. Phys. 77, 189
Dere K.P., Mason H.E., Widing K.G., Bhatia A.K., 1979, ApJS 40, 341
Doschek G.A., Feldman U., Van Hoosier M.E., Bartoe J.D.F., 1976, ApJS 31, 417
Dufton P.L., Kingston A.E., Widing K.G., 1990, ApJ 353, 323
Edlén B., 1942, Z. Ap. 22, 30
Eissner W., Galavís M.E., Mendoza C., Zeippen C.J., 1999, A&AS (in press)
Eissner W., Jones M., Nussbaumer H., 1974, Comput. Phys. Commun. 8, 270
Eissner W., Nussbaumer H., 1969, J. Phys. B 2, 1028
Feldman U., Laming J.M., Mandelbaum P., Goldstein W.H., Osterheld A., 1992, ApJ 398, 692
Hummer D.G., Berrington K.A., Eissner W., Pradhan A.K., Saraph H.E., Tully J.A., 1993, A&A 279, 298
Kastner S.O., Mason H.E., 1978, A&A 67, 119
Keenan F.P., Dufton P.L., Conlon E.S., Foster V.J., Kingston A.E., Widing K.G., 1993, ApJ 405, 798
Litzén U., Redfors A., 1987, Phys. Scr. 36, 895
Mann J.B., 1983, At. Data Nucl. Data Tab. 29, 407
Mason H.E., 1975, MNRAS 170, 651
Mendoza C., 1999, Comput. Phys. Commun. (in press)
Neupert W.M., Brosius J.W., Thomas R.J., Thompson W.T., 1992, ApJ 392, L95
Nussbaumer H., Storey P.J., 1978, A&A 64, 139
Pradhan A.K., 1988, At. Data Nucl. Data Tab. 40, 335
Redfors A., 1988, Phys. Scr. 38, 702
Schmitt J.H.M.M., Drake J.J., Stern R.A., Haisch B.M., 1996, ApJ 457, 882
Scott N.S., Burke P.G., 1980, J. Phys B 12, 4299
Scott N.S., Taylor K.T., 1982, Comput. Phys. Commun. 25, 349
Seaton M.J., 1985, J. Phys. B 18, 2111
Stern R.A., Lemen J.R., Schmitt J.H.M.M., Pye J.P., 1995, ApJ 444, L45
Thomas R.J., Neupert W.M., 1994, ApJS 91, 461
Vernazza J.E., Reeves E.M., 1978, ApJS 37, 485
Widing K.G., Cook J.W., 1987, ApJ 320, 913